

Detection of Nucleosomal Substructures using Solid-State Nanopores

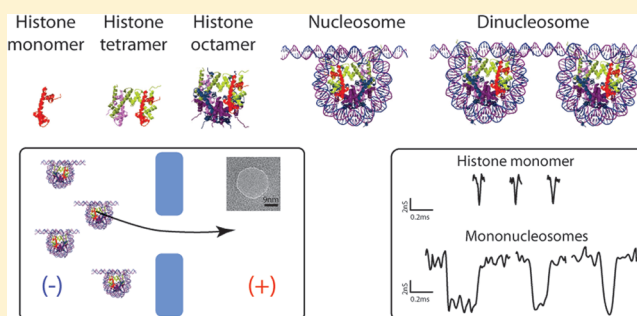
Gautam V. Soni and Cees Dekker*

Department of Bionanoscience, Kavli Institute of Nanoscience, Delft University of Technology, Lorentzweg 1, 2628 CJ Delft, The Netherlands

S Supporting Information

ABSTRACT: Histone proteins assemble onto DNA into nucleosomes that control the structure and function of eukaryotic chromatin. More specifically, the structural integrity of nucleosomes regulates gene expression rates and serves as an important early marker for cell apoptosis. Nucleosomal (sub)structures are however hard to detect and characterize. Here, we show that solid-state nanopores are well suited for fast and label-free detection of nucleosomes and its histone subcomplexes. (Nucleo-)protein complexes are individually driven through the nanopore by an applied electric field, which results in characteristic conductance blockades that provide quantitative information on the molecular size of the translocating complex. We observe a systematic dependence of the conductance blockade and translocation time on the molecular weight of the nucleosomal substructures. This allows discriminating and characterizing these protein and DNA-protein complexes at the single-complex level. Finally, we demonstrate the ability to distinguish nucleosomes and dinucleosomes as a first step toward using the nanopore platform to study chromatin arrays.

KEYWORDS: Nanopore, nucleosomes, histone oligomers, dinucleosomes, molecular volume, single molecule



Nucleosomes are dynamic structures of fundamental importance in DNA packaging and DNA-based cellular processes such as transcription, replication, and repair.^{1,2} In a nucleosome, four types of histone proteins (H2A, H2B, H3, and H4) come together in a hierarchical fashion. Two copies each of H3 and H4 proteins bind to form a (H3–H4)₂ tetramer to which two H2A–H2B dimers bind to in order to complete the octamer. About 146 base pairs (bp) of DNA tightly wraps around the positively charged core of histone octamer to form the complete nucleosome.³ Nucleosomes have two primary functions: first, to structurally package DNA to fit into the cell nucleus, and second, to regulate gene expression by controlling the DNA accessibility to the genetic machinery such as polymerases and transcription factors.

Structural reorganization (assembly, partial disintegration into subcomplexes or complete removal) of nucleosomes and histones oligomers (histone monomers, dimers, tetramers, and octamers) is essential for chromatin dynamics.^{4,5} Changes in stoichiometry of histone complexes and nucleosomes are involved in a wide variety of cellular processes from controlling gene expression patterns to regulating progression of cell apoptosis. There is a multitude of reasons why one would like to accurately detect nucleosomal substructures. Inside the cell nucleus, histone oligomers are extensively exchanged on highly active genes.⁶ This dissociation and association of histone oligomers from/to nucleosomes occurs both spontaneously and with the aid of ATP-driven chromatin remodelers and histone

chaperones. The thermodynamic and kinetic description of nucleosome assembly and unfolding depends on the relative abundance of the various types of histone oligomers in the cell nucleus.^{7–12} Accumulation of histones and nucleosomes in cell lysates, for example, in human lymphoblasts,^{13,14} has been shown to be early markers of cell death. Rapid and sensitive detection of histone oligomers and nucleosomes is essential to mark these early signatures of autoimmune diseases like systemic lupus erythematosus.¹⁵ An important result of the dynamic un/refolding of nucleosomes is the mixed population of fully and partially formed nucleosomes on chromatin that collectively modulate actively transcribed or repressed states of a particular gene region. A detection method to measure patterns of nucleosomal substructures along a gene is currently unavailable.

Western blots, ELISA, and gel-shift electrophoresis^{16–18} are widely used to detect and analyze histone proteins. These methods require large sample volumes as well as labeled secondary antibodies to achieve a measurable contrast between different protein complexes. Fluorescence of labeled histones and nucleosomes in solution^{19–21} has been used to study their diffusion properties but this requires either specific fluorophore labeling of purified histones or genetic manipulation of cell lines

Received: March 26, 2012

Revised: April 18, 2012

Published: May 4, 2012

to add fluorescent protein tag to histones.^{22,23} AFM imaging can also be used to study nucleosome and chromatin fibers but these scanning-probe results suffer from uncertainties caused by the proximity of the deposition surface that are particularly pronounced for histones and nucleosomes. Here we present solid-state nanopores as a novel method to detect nucleosomes and its substructures down to the single-molecule level. Nanopores provide a fast, sensitive and label-free detection platform to detect histone oligomers and nucleosomes, which opens doors to study early apoptotic markers as well as higher-order chromatin structure.

A nanopore is a nanometer-size hole in a thin solid-state membrane. When assembled in a flow cell, the membrane divides the ionic buffer solution into two chambers with the pore being the only opening that connects the fluids on its either side. Under an applied potential, ions that flow from one side of the membrane to the other through the pore are measured as open pore current. Biological molecules (DNA, proteins, protein complexes, or DNA–protein assemblies) are charged macromolecules that translocate through the pore under the applied voltage (see Figure 1b). Translocation of

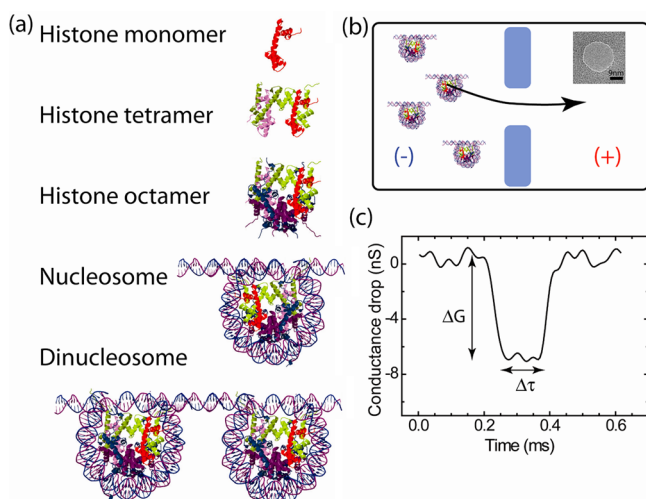


Figure 1. (a) Schematic of the histone oligomers and nucleosome assemblies investigated in this study. (b) Schematic of a typical translocation experiment using a 20 nm pore in silicon nitride membrane. Inset shows a TEM image of a 20 nm nanopore. (c) Example of a typical blockade event due to translocation of a histone octamer, indicating the conductance blockade (ΔG) and dwell time ($\Delta \tau$).

single biomolecules through the nanopores is detected as transient blockade events in the pore conductance. These events are characterized in terms of the depth of conductance blockade, ΔG , and its duration, the dwell time, $\Delta \tau$ (see Figure 1c).²⁴ These translocation events are characteristic of the molecular size and charge of the translocating biomolecule. Statistical analysis of many hundreds of these single-molecule translocation events is used to distinguish and characterize biomolecular populations of different molecular sizes. Nanopores have proven to be excellent at detecting DNA, proteins and recently protein–DNA complexes at the single molecule level.^{25–28} Here, we use solid-state nanopores to detect nucleosomes and differentiate them from subtly distinct nucleosomal substructures.

Figure 1a shows the schematic of the various protein complexes and DNA–protein assemblies that are investigated

in this work, namely, histone monomers, $(H3-H4)_2$ tetramers, $(H2A-H2B-H3-H4)_2$ histone octamers, mononucleosomes made on 344bp DNA with one “601” nucleosome positioning sequence, and dinucleosomes made on 1027bp DNA with one 601 nucleosome positioning sequence. The histone monomers and complexes are positively charged, whereas the DNA–histone assemblies (mono- and dinucleosomes) have a net negative charge. For translocation experiments, sample is added in the chamber with appropriate polarity, where the molecule of interest is driven through the pore electrophoretically.

Nucleosomes were assembled by a slow dialysis of DNA with histone octamers as indicated in Figure 2a (see Methods for details).^{29,30} To optimize assembly conditions and maximize the yield of fully assembled nucleosomes, it was important to do a careful titration of the DNA to histone–octamer molar ratio, as shown in Figure 2b. The fully assembled nucleosomes were purified from free DNA and histone proteins by fractionating on a glycerol gradient (see Methods). Figure 2c shows a 6% PAGE gel of purified nucleosomes, demonstrating a high yield. To form dinucleosomes, 1027bp DNA with a single nucleosome positioning 601 sequence was used. DNA and histone octamers were assembled with molar ratio of 1:2. After assembly, DNA with zero, one (mononucleosomes), or two (dinucleosomes) nucleosomes were separated by fractionating on a glycerol gradient. Purified sample was inspected by gel electrophoresis. Figure 2d shows 0.8% agarose gel of the fractionated samples. Fractions containing only dinucleosomes were pooled and concentrated using 100 kDa centrifuge filters. These purified nucleosome/dinucleosome samples were stored at 4 °C and used as is in nanopore translocation experiments. We verified the stability of nucleosomes in our experimental buffer containing 1 M KCl for the duration of a typical translocation experiment (20 min) by gel electrophoresis. Upon incubation in buffers with 0.2 to 1 M KCl, nucleosomes were found to either be fully complexed or disintegrate completely into histones and DNA in an all-or-none process. No DNA-bound partial histone complexes were detected by gel electrophoresis (see Supporting Information, Figure S1). Importantly, during translocation of nucleosomes, only the negatively charged assemblies will be electrophoretically driven through the pore whereas the positively charged free histone protein and histone complexes will be pushed away from the pore. Finally, we note that translocation of the relatively small (344bp and 1027bp) free DNA through a 20 nm diameter pore is practically invisible within the time resolution (~ 100 kHz) of our experiments.^{31,32}

Upon addition of histone oligomers or nucleosomes to the nanopore chamber, we detect transient current blockade events that signal the translocation of individual complexes. Such measurements yield important information about the translocating molecule in particular its molecular volume. Figure 3a shows typical conductance blockade events for histone monomers and nucleosome complexes. Depending on the translocating complex, we see clear blockade events with a ΔG of 3–10 nS and dwell times of 0.1–0.5 ms, that are well distinguishable from the noise of open pore current baseline. We observe that the structurally smaller histone proteins display shorter dwell times as well as smaller conductance blockades (Figure 3a top row) when compared to translocation events of fully assembled nucleosomes (Figure 3a bottom row). Many hundreds of these events are used to quantitatively analyze their statistical characteristics. Figure 3b shows a scatter plot of 1250 events with conductance blockades that signal the

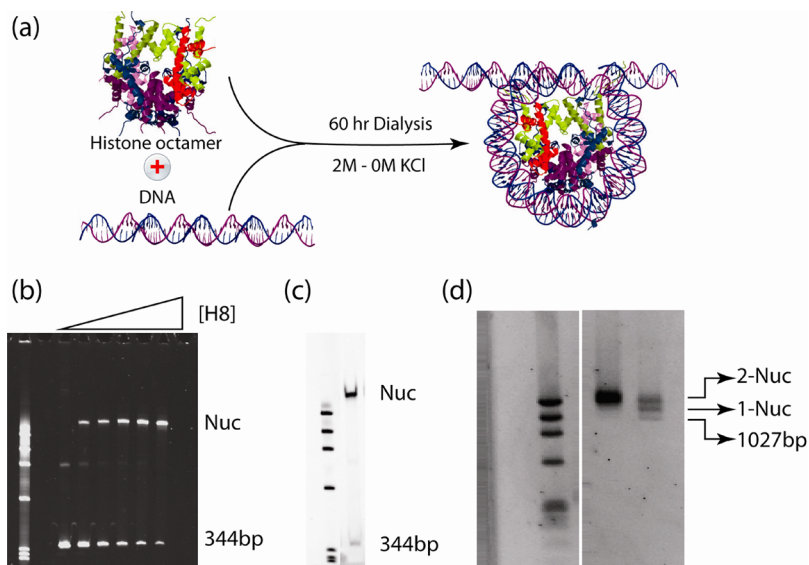


Figure 2. Nucleosome assembly on 344bp DNA. (a) Schematic of nucleosome assembly procedure. (b) Dependence of the yield of nucleosome assembly on histone octamer concentration. Lane 1, marker; Lane 2, blank; Lane 3, control DNA (344bp DNA); Lanes 4–8, [octamer]/[DNA] ratio of 0.6, 0.8, 0.9, 1.0, and 1.2, respectively. For all subsequent experiments, a ratio of 1.2 was used. (c) Purification of assembled nucleosomes over a 10–30% glycerol gradient. Lane 1, marker. Lane 2, purified mononucleosomes. (d) Agarose gel (0.8%) showing bare DNA (1027bp) and DNA with 1 or 2 nucleosomes, labeled as 1-Nuc and 2-Nuc respectively. Lane 1, marker. Lane 2, pooled fractions of purified dinucleosomes. Lane 3, mix of bare 1027bp DNA, DNA with 1 and DNA with 2 nucleosomes, as indicated by the arrows.

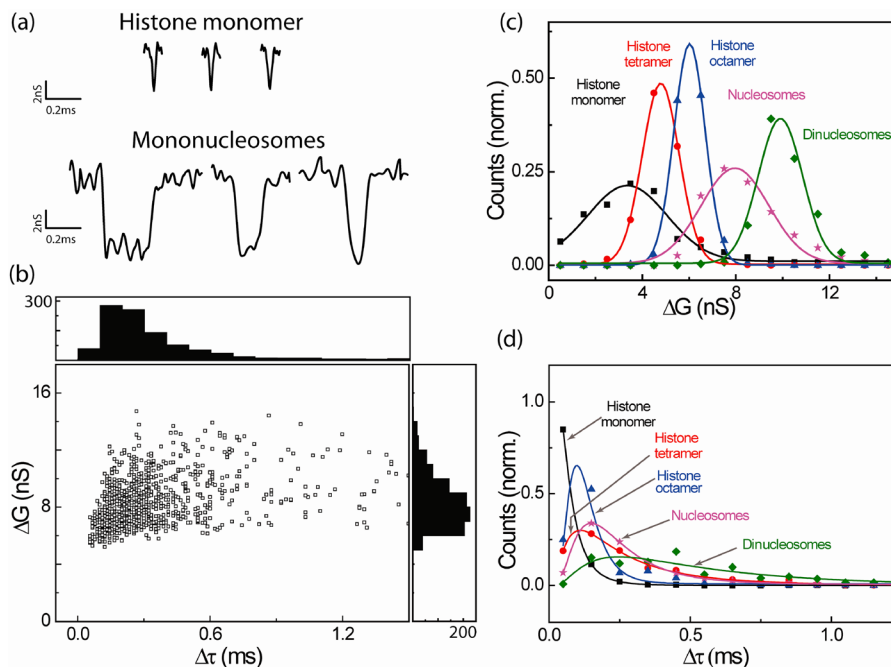


Figure 3. Translocation of nucleosomal substructures. (a) Typical translocation events of histone monomers (top) and mononucleosomes (bottom) through a 20 nm pore at 100 mV applied across the pore. (b) Scatter plot of mononucleosome translocations events ($N = 1250$). ΔG and $\Delta\tau$ histograms are plotted on the right and top, respectively. (c) Conductance blockade (ΔG) histograms of histone monomers (black, squares), histone tetramers (red, circles), histone octamers (blue, triangles), mononucleosomes (magenta, stars), and dinucleosomes (green, diamonds). For comparison all histograms are normalized by the total number of counts. Solid lines are Gaussian fits to the histograms. (d) Dwell time ($\Delta\tau$) histograms of translocation events for histone monomers (black, squares), histone tetramers (red, circles), histone octamers (blue, triangles), mononucleosomes (magenta, stars), and dinucleosomes (green, diamonds). Solid lines are log-normal fits to the histograms.

translocation of individual nucleosome molecules through a 20 nm diameter nanopore. In such a scatter plot, the conductance blockade ΔG is plotted against the dwell time $\Delta\tau$ of individual events. Corresponding histograms of ΔG and $\Delta\tau$ are shown to the right and top of Figure 3b, respectively. We confirmed translocation of mononucleosomes through the nanopore by

monitoring “recaptured” translocation events³³ when the potential was reversed. All measurements were done in identical experimental buffer (10 mM Tris, 1 mM EDTA, and 1 M KCl) with 100 mV applied potential across 20 nm diameter silicon nitride nanopores.

Table 1. Calculation of Molecular Volumes of Translocating Biomolecule through the Nanopore^a

molecule	molecular weight (kDa)	$\Delta\tau$ (most probable, ms)	ΔG (nS)	molecular volume (nm ³) (calculated from ΔG)
histone monomer	13.56	0.03 (−0.02/+0.04)	3.4 ± 1.7	275 ± 138
histone tetramer	53.02	0.11 (−0.07/+0.18)	4.8 ± 0.8	389 ± 64
histone octamer	108.5	0.10 (−0.04/+0.07)	6.0 ± 0.7	473 ± 57
nucleosome	335.53	0.15 (−0.08/+0.16)	8.0 ± 1.4	509 ± 89
dinucleosome	894.8	0.25 (−0.15/+0.39)	9.9 ± 0.9	801 ± 76

^aThe complexes studied and their molecular weights are listed in columns 1 and 2 respectively. Column 3 has the most probable dwell time as estimated by lognormal fits to the $\Delta\tau$ distributions. The hwhm spread of these distributions is listed as errors in parentheses. Mean ΔG is listed in Column 4 with standard deviations as error bars. Column 5 lists the calculated molecular volume from ΔG values (see text). The shape factor γ was estimated to be 1.9 for mononucleosomes ($a = 6, b = 10$) and 1.54 for histone octamer ($a = 6, b = 6.4$) by assuming them to be oblate spheroids. For rest of complexes, γ was set to 1.5, value as expected for spheroids.

We next quantitatively compare histograms of conductance blockades ΔG of the five different molecular complexes that we have investigated. For each complex, we measured hundreds of translocation events and the corresponding ΔG histograms are shown in Figure 3c. For example, translocation of mononucleosomes through a 20 nm pore yields a ΔG of 8.0 ± 1.5 nS, where the error bar denotes the standard deviation of the fitted Gaussian distribution. These values were found consistent when measured in 12 different 20 nm diameter pores, demonstrating the repeatability of this method. Similarly, ΔG distributions from translocations of histone monomers, tetramers, and octamers were measured, as shown. The mean ΔG values from these distributions are listed in Table 1. Interestingly, we note that the order of the peak maxima of conductance blockades histograms follows the order of the molecular sizes.

From the conductance drops in nanopore current, we can estimate the molecular volume of the translocating complexes. Unlike for most nanopores experiments on DNA, the nucleosomes are smaller than the height of the nanopore (the thickness of silicon nitride membrane is 20 nm). The conductance blockade is therefore proportional to the volume of ionic solution excluded from the nanopore by the molecular volume of the complex (not its crosssection). The drop in open pore conductance due to excluded volume of the translocating nucleosome can be estimated by the following expression^{34,35}

$$\Delta G = \gamma\sigma \frac{V_{\text{excluded}}}{\left(h_p + \frac{\pi}{4}d_p\right)^2} f(d_p, d_m) \quad (1)$$

where V_{excluded} is the ionic volume excluded by the translocating protein complex, γ is the shape factor³⁶ of nucleosomes, $\sigma = 10.5$ S/m at 23 °C³⁷ is the bulk conductivity of 1 M KCl, h_p and d_p are height and diameter of pore, respectively (both fixed at a value of 20 nm), and f is a correction factor that depends on the relative values of pore diameter and the diameter of molecule, d_m . We adopt a value of $f = 1$, as commonly used in literature.^{35,38–40} We estimate that $\gamma = 1.9$ by approximating a nucleosome as oblate spheroid of principal axes (a,b,b) with $a = 6$ nm and $b = 10$ nm. Using the measured mean ΔG of nucleosomes, we can subsequently estimate the molecular volume of translocating nucleosome to be $V_{\text{Nucleosome}} = 509 \pm 89$ nm³. This is in very good agreement with the value of 532 nm³ for the nucleosome volume as measured by X-ray crystallography^{3,41} and 580 nm³ as measured by atomic force microscopy (AFM).^{42,43} Comparing ΔG histograms of each molecule and following a similar calculation, we can estimate the molecular volumes of each of these histone oligomers. We list these calculated values in Table 1 along with their molecular

weights. Monomeric histone proteins are the smallest in size (275 nm³), followed in increasing order by histone tetramers, histone octamers, and finally the mononucleosomes and dinucleosomes (801 nm³). We find, as expected, that the larger the molecular size of the complex, the deeper the conductance blockade during translocation. This is quantitatively shown in Figure 4a, which displays the monotonous increase of ΔG with the molecular mass of the protein complex.

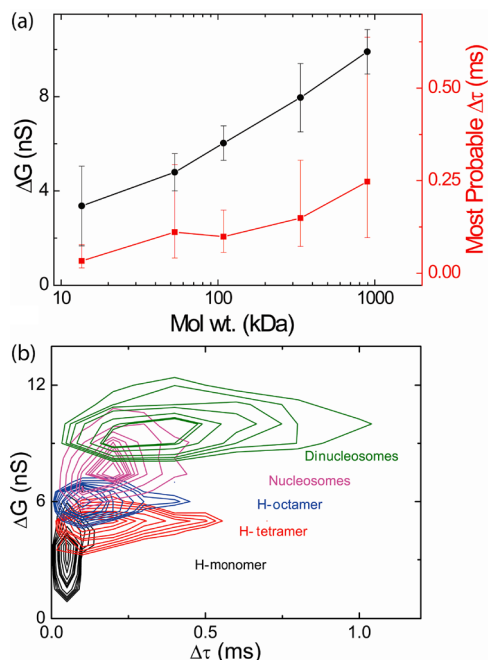


Figure 4. (a) Mean conductance blockades, ΔG (black circles, left axis) and most probable dwell times, $\Delta\tau$ (red squares, right axis) are plotted against molecular weight of the various complexes. (b) Scatter plots of conductance blockades (ΔG) versus dwell times ($\Delta\tau$) of all the different assemblies studied. The distributions are plotted as contour plots for clarity (for full scatter plots with all separate data points, see Supporting Information). Histone monomers (black), histone tetramers (red), histone octamers (blue), mononucleosomes (magenta), and dinucleosomes (green). All molecular species can be well separated based on ΔG or $\Delta\tau$.

Next we compare the statistics of the dwell times of these complexes. In Figure 3d, we show the dwell time histogram for nucleosomes and compare them to dwell times for various histone oligomers. We find that the dwell time histograms are well fit by a log-normal distribution (i.e., a Gaussian on a log scale). For nucleosomes, a most probable dwell time $\Delta\tau$ of 0.15 (−0.08/+0.16) ms was measured, where the error denotes the

half width and half-maximum (hwhm) of the distribution. This value is much larger than the $\sim 4 \mu\text{s}$ dwell time anticipated for a bare 344bp DNA under similar solvent conditions as estimated by the power-law dependence of dwell time on DNA length that was measured previously.⁴⁴ From the translocation across the 20 nm nanopore height in a dwell time of 0.15 ms, we estimate a typical mean speed of about $135 \mu\text{m/s}$. This velocity is about ~ 40 times slower than that of the estimated mean velocity of bare 344bp dsDNA ($\sim 5 \text{ mm/sec}$). This slowing down of nucleosomes can be attributed to two effects: first, when moving under the applied potential, the bulky disk-shaped nucleosomes will experience a higher fluidic drag when compared to a bare dsDNA. Second, and likely most important, nucleosomes contain a positively charged histone protein core leading to a lower net charge density than bare dsDNA, thus retarding the translocation speed in electrophoresis.⁴⁵ Figure 3d compares the dwell time histograms of nucleosomes with its histone protein subcomplexes. We find that histone complexes translocate faster than mononucleosomes. For each distribution, we estimate the most probable time of translocation by fitting with a log-normal distribution. We find that the most probable dwell time ranges from $\Delta\tau \sim 30 \mu\text{s}$ for histone monomers to $\Delta\tau \sim 100 \mu\text{s}$ for histone octamers, see Table 1. Interestingly, even with the complex charge distributions and shape differences in these protein and DNA–protein assemblies, we find a systematic dependence where the larger the size of the biomolecular complex traversing through the pore, the longer the corresponding dwell times (see Figure 4a).

Next, as a first step in the direction of measuring on nucleosome arrays, we compare translocation of mononucleosomes to that of dinucleosomes, which is a linear array of two nucleosomes. Figure 3c (green diamonds) compares the conductance blockade of dinucleosomes with the ΔG histograms of all other assemblies. For dinucleosomes, we measure mean ΔG of $9.9 \pm 0.9 \text{ nS}$. Using a similar analysis as in the case of mononucleosomes and histone oligomers, we estimate the molecular volume of dinucleosomes that occludes ionic conduction of nanopore to be 801 nm^3 , which is a factor of 1.6 higher than that measured for mononucleosomes (see Table 1). A similar distinction between mono- and dinucleosomes is visible when we also consider the dwell times ($\Delta\tau$ -histograms, Figure 3d). The most probable translocation time of dinucleosomes was measured to be $250 \mu\text{s}$, a factor of ~ 1.7 higher than that measured for mononucleosomes.

We can understand the difference between the translocation characteristics of mono- and dinucleosomes based on their structural features. Because of its overall larger molecular size, dinucleosomes translocate slower through the nanopore as compared to mononucleosomes. Mono- and dinucleosome assemblies differ in their lengths. Within the 1027bp long DNA used in assembling dinucleosomes, one nucleosome binds to the single nucleosome positioning 601 sequence while the other is randomly placed on the remainder of the DNA. Each complex has 147bp of DNA wrapped around it, leaving 733bp of free dsDNA which corresponds to a contour length of about 250 nm. Dinucleosomes can thus translocate through the pore in a linear configuration, which would yield a similar ΔG and longer $\Delta\tau$ than the values for mononucleosomes, or in a configuration where the free DNA (partly) folds back on the nucleosomes, giving rise to a larger cross section and a higher ΔG . The larger value for ΔG that we observe for dinucleosomes provides evidence for the latter. By comparing

the translocation events on a two-dimensional parameter space of ΔG and $\Delta\tau$, populations of mono- and dinucleosomes can be well distinguished. This indicates that nanopore studies bear potential for rapid characterization of arrays of nucleosomes.

In Figure 4b, we finally show scatter plots where the conductance blockades are plotted against the dwell times for all the complexes in our study. For clarity, we show these scatter plots as isodensity contour lines of the data (see Supporting Information for scatter plots with all data points, Supporting Information Figure S2). We clearly see the different molecular complexes separated as different populations. Histone monomers form the population at the left-bottom corner with the smallest dwell times and lowest conductance blockades. Histone tetramers, octamers, and nucleosomes have similar dwell times but these complexes can be well separated based on their different conductance blockades. Finally, mono- and dinucleosomes are distinguished based on conductance blockades but more importantly on the translocation dwell times. These measurements demonstrate the ability of the nanopore platform to distinguish between subtle structural differences in various subnucleosomal complexes.

In conclusion, we present here the first report on translocation of nucleosomes and its substructures through solid-state nanopores. Under an applied potential, we translocate histone oligomers and nucleosomes through 20 nm diameter silicon nitride nanopores. Analysis of the translocation events revealed conductance blockades and dwell times that are characteristic of the complex under study. From the mean conductance blockades, we estimated molecular volumes of the protein, protein complex or DNA–protein assembly traversing through the pore. We find that larger complexes lead to deeper conductance blockades and longer translocation times. By characterizing translocation events on a 2D parameter space of conductance blockade and dwell time parameters, we showed a clear distinction of populations of histone monomers, tetramers, and octamers. This was furthermore realized for mono- and dinucleosomes, which shows that this approach can be expanded to study larger nucleosome arrays. From a practical perspective, our findings of fast and sensitive characterization of nucleosomes and histone oligomers open up new avenues for early detection of apoptotic states and cancer markers in blood plasma of patients. Our findings also provides the possibility of sensing nucleosome positioning on chromatin fibers by controlled threading of nucleosomal arrays into a nanopore using, for example, an integrated optical tweezers. Overall, the data show that nanopores are a new platform to differentiate subnucleosomal structures, providing a new way to study chromatin at the single-molecule level.

Methods. Nucleosome Preparation. Histone octamers and tetramers (chicken erythrocyte) were purchased from Abcam (Abcam, MA USA). The 344bp and 1027bp DNA with a 601 nucleosome positioning sequence was extracted from pGEM plasmid (gift from Widom lab). Histone monomers (H2A, H2B, H3, and H4, a gift from the P. Verrijzer lab) were purified from *Drosophila* and stored at $4 \text{ }^\circ\text{C}$ at subnanomolar concentrations to reduce any nonspecific aggregation. Nucleosomes were reconstituted by mixing DNA and histone octamers at appropriate molar ratio (1:1.2 for mononucleosomes on 344bp DNA and 1:2 for dinucleosomes on 1027bp DNA) in high salt buffer (2 M KCl, 20 mM Tris-HCl, 1 mM EDTA, pH 7.5, 1 mM DTT, and 0.5 mM benzamidine) and lowering the ionic strength in a 60 h dialysis against a low salt buffer (250 mM KCl, 10 mM Tris-HCl, 1 mM EDTA, 1 mM

DTT, and 0.5 mM benzamidine). Finally the nucleosomes were dialyzed against TCS buffer (20 mM Tris-HCl, 1 mM EDTA, and 1 mM DTT) for at least 4 h.^{29,30} Reconstituted nucleosomes and dinucleosomes were purified from free proteins and DNA by fractionating in 10–30% glycerol gradient for 16.5 h at 35 000 rpm. Nucleosome containing fractions were pooled and checked by running 6% PAGE gel (stained for 20 min in SybrGold, Invitrogen) and stored at 4 °C.

Nanopore Experiments. Silicon wafers with a triple layer consisting of 20 nm silicon nitride, 100 nm silicon oxide, and 500 nm silicon nitride were processed with standard optical and e-beam lithography to fabricate free-standing silicon nitride membranes (with a window of 5 μm diameter and 20 nm thickness). A focused TEM beam was used to drill 20 nm pores in these membranes.^{46–48} These nanopores were mounted in a fluid cell separating the cis and trans chambers filled with buffer (1 M KCl, 10 mM Tris-EDTA, pH8). All experiments were performed at on 20 nm pores at 100 mV bias voltage applied across the nanopore membrane using Ag/AgCl electrodes. Nanopore current was measured using Axopatch 200B (Axon Instruments) set at full bandwidth (100 kHz). A 0.1–1 pM sample was introduced in the flow chamber and events were observed. Low-sample concentrations ensured reduction in pore clogging and aggregation of proteins. Data was recorded using a DAQ card (NI-PCI 6251, National Instruments) at acquisition rate of 200 kHz. For analysis, data was filtered at 35 kHz. All data acquisition and event detection in current traces was done by custom written software in LabVIEW (National Instruments).^{44,49}

■ ASSOCIATED CONTENT

■ Supporting Information

Details of stability of nucleosomes in buffers with different salt concentrations and scatter plot of conductance blockade plotted against dwell times for histone monomers, tetramers, octamers, and mono- and dinucleosomes. This material is available free of charge via the Internet at <http://pubs.acs.org>.

■ AUTHOR INFORMATION

Corresponding Author

*E-mail: c.dekker@tudelft.nl.

Notes

The authors declare no competing financial interest.

■ ACKNOWLEDGMENTS

We thank M. Y. Wu for contributions to nanopore fabrication, S. Hage and B. Cross for help with biochemistry, and Rifka Vlijm for valuable discussions. This work is supported by ERC-2009-AdG Grant NANOforBIO.

■ REFERENCES

- (1) Wolffe, A. P.; Kurumizaka, H. *Prog. Nucleic Acid Res. Mol. Biol.* **1998**, *61*, 379–422.
- (2) Workman, J. L.; Kingston, R. E. *Annu. Rev. Biochem.* **1998**, *67*, 545–79.
- (3) Luger, K.; Mader, A. W.; Richmond, R. K.; Sargent, D. F.; Richmond, T. J. *Nature* **1997**, *389* (6648), 251–260.
- (4) Bohm, V.; Hieb, A. R.; Andrews, A. J.; Gansen, A.; Rocker, A.; Toth, K.; Luger, K.; Langowski, J. *Nucleic Acids Res.* **2011**, *39* (8), 3093–3102.
- (5) Widom, J. *Annu. Rev. Biophys. Biomol. Struct.* **1998**, *27*, 285–327.

- (6) Katan-Khaykovich, Y.; Struhl, K. *Proc. Natl. Acad. Sci. U.S.A.* **2011**, *108* (4), 1296–301.
- (7) Van Holde, K. E. *Chromatin*; Springer-Verlag: New York, 1989.
- (8) Jackson, V. *Biochemistry* **1990**, *29* (3), 719–31.
- (9) Wolffe, A. P. *Chromatin: Structure and Function*, 3rd ed.; Academic Press: New York, 1998.
- (10) Banks, D. D.; Gloss, L. M. *Biochemistry* **2003**, *42* (22), 6827–39.
- (11) Andrews, A. J.; Luger, K. *Methods Enzymol.* **2011**, *488*, 265–285.
- (12) Andrews, A. J.; Luger, K. *Annu. Rev. Biophys.* **2011**, *40* (40), 99–117.
- (13) Wu, D.; Ingram, A.; Lahti, J. H.; Mazza, B.; Grenet, J.; Kapoor, A.; Liu, L.; Kidd, V. J.; Tang, D. J. *Biol. Chem.* **2002**, *277* (14), 12001–8.
- (14) Gabler, C.; Blank, N.; Hieronymus, T.; Schiller, M.; Berden, J. H.; Kalden, J. R.; Lorenz, H. M. *Ann. Rheum. Dis.* **2004**, *63* (9), 1135–44.
- (15) van Nieuwenhuijze, A. E.; van Lopik, T.; Smeenk, R. J.; Aarden, L. A. *Ann. Rheum. Dis.* **2003**, *62* (1), 10–4.
- (16) Chavez-Blanco, A.; Segura-Pacheco, B.; Perez-Cardenas, E.; Taja-Chayeb, L.; Cetina, L.; Candelaria, M.; Cantu, D.; Gonzalez-Fierro, A.; Garcia-Lopez, P.; Zambrano, P.; Perez-Plasencia, C.; Cabrera, G.; Trejo-Becerril, C.; Angeles, E.; Duenas-Gonzalez, A. *Mol. Cancer* **2005**, *4* (1), 22.
- (17) Shechter, D.; Dormann, H. L.; Allis, C. D.; Hake, S. B. *Nat. Protoc.* **2007**, *2* (6), 1445–57.
- (18) Kizer, K. O.; Xiao, T.; Strahl, B. D. *Methods* **2006**, *40* (4), 296–302.
- (19) Visnapuu, M. L.; Greene, E. C. *Nat. Struct. Mol. Biol.* **2009**, *16* (10), 1056–62.
- (20) Tomschik, M.; Zheng, H.; van Holde, K.; Zlatanova, J.; Leuba, S. H. *Proc. Natl. Acad. Sci. U.S.A.* **2005**, *102* (9), 3278–83.
- (21) Gansen, A.; Valeri, A.; Hauger, F.; Felekyan, S.; Kalinin, S.; Toth, K.; Langowski, J.; Seidel, C. A. *Proc. Natl. Acad. Sci. U.S.A.* **2009**, *106* (36), 15308–13.
- (22) Bhattacharya, D.; Mazumder, A.; Miriam, S. A.; Shivashankar, G. V. *Biophys. J.* **2006**, *91* (6), 2326–36.
- (23) Kimura, H.; Cook, P. R. *J. Cell Biol.* **2001**, *153* (7), 1341–53.
- (24) Dekker, C. *Nat. Nanotechnol.* **2007**, *2* (4), 209–215.
- (25) Firnkes, M.; Pedone, D.; Knezevic, J.; Doblinger, M.; Rant, U. *Nano Lett.* **2010**, *10* (6), 2162–2167.
- (26) Kowalczyk, S. W.; Hall, A. R.; Dekker, C. *Nano Lett.* **2010**, *10* (1), 324–328.
- (27) van den Hout, M.; Skinner, G. M.; Klijnhout, S.; Krudde, V.; Dekker, N. H. *Small* **2011**, *7* (15), 2217–2224.
- (28) Wanunu, M.; Sutin, J.; McNally, B.; Chow, A.; Meller, A. *Biophys. J.* **2008**, *95* (10), 4716–4725.
- (29) Dyer, P. N.; Edayathumangalam, R. S.; White, C. L.; Bao, Y.; Chakravarthy, S.; Muthurajan, U. M.; Luger, K.; Allis, C. D.; Carl, W. Reconstitution of Nucleosome Core Particles from Recombinant Histones and DNA. *Methods Enzymol.* **2003**, *375*, 23–44.
- (30) Lee, K. M.; Narlikar, G. *Curr. Protoc. Mol. Biol.* **2001**, Chapter 21, Unit 21 6.
- (31) Smeets, R. M. M.; Keyser, U. F.; Krapf, D.; Wu, M. Y.; Dekker, N. H.; Dekker, C. *Nano Lett.* **2006**, *6* (1), 89–95.
- (32) Smeets, R. M. M.; Keyser, U. F.; Dekker, N. H.; Dekker, C. *Proc. Natl. Acad. Sci. U.S.A.* **2008**, *105* (2), 417–421.
- (33) Gershow, M.; Golovchenko, J. A. *Nat. Nanotechnol.* **2007**, *2* (12), 775–9.
- (34) Talaga, D. S.; Li, J. L. *J. Am. Chem. Soc.* **2009**, *131* (26), 9287–9297.
- (35) Yusko, E. C.; Johnson, J. M.; Majd, S.; Prangko, P.; Rollings, R. C.; Li, J.; Yang, J.; Mayer, M. *Nat. Nanotechnol.* **2011**, *6* (4), 253–60.
- (36) Grover, N. B.; Naaman, J.; Ben-Sasson, S.; Doljanski, F. *Biophys. J.* **1969**, *9* (11), 1398–414.
- (37) Haynes, W. M. *CRC Handbook of Chemistry and Physics*, 91st ed.; CRC Press: Boca Raton, FL, 2010.
- (38) Ito, T.; Sun, L.; Crooks, R. M. *Anal. Chem.* **2003**, *75* (10), 2399–406.

- (39) Raillon, C.; Cousin, P.; Traversi, F.; Garcia-Cordero, E.; Hernandez, N.; Radenovic, A. *Nano Lett.* **2012**, *12* (3), 1157–64.
- (40) Han, A.; Creus, M.; Schurmann, G.; Linder, V.; Ward, T. R.; de Rooij, N. F.; Staufer, U. *Anal. Chem.* **2008**, *80* (12), 4651–8.
- (41) Richmond, T. J.; Finch, J. T.; Rushton, B.; Rhodes, D.; Klug, A. *Nature* **1984**, *311* (5986), 532–7.
- (42) Pisano, S.; Leoni, D.; Galati, A.; Rhodes, D.; Savino, M.; Cacchione, S. *Nucleic Acids Res.* **2010**, *38* (7), 2247–55.
- (43) Yoda, K.; Ando, S.; Morishita, S.; Houmura, K.; Hashimoto, K.; Takeyasu, K.; Okazaki, T. *Proc. Natl. Acad. Sci. U.S.A.* **2000**, *97* (13), 7266–71.
- (44) Storm, A. J.; Storm, C.; Chen, J.; Zandbergen, H.; Joanny, J. F.; Dekker, C. *Nano Lett.* **2005**, *5* (7), 1193–7.
- (45) Wanunu, M.; Sutin, J.; Meller, A. *Nano Lett.* **2009**, *9* (10), 3498–3502.
- (46) Wu, M. Y.; Smeets, R. M. M.; Zandbergen, M.; Ziese, U.; Krapf, D.; Batson, P. E.; Dekker, N. H.; Dekker, C.; Zandbergen, H. W. *Nano Lett.* **2009**, *9* (1), 479–484.
- (47) van den Hout, M.; Hall, A. R.; Wu, M. Y.; Zandbergen, H. W.; Dekker, C.; Dekker, N. H. *Nanotechnology* **2010**, *21* (11), 115304.
- (48) Storm, A. J.; Chen, J. H.; Ling, X. S.; Zandbergen, H. W.; Dekker, C. *Nat. Mater.* **2003**, *2* (8), 537–540.
- (49) Storm, A. J.; Chen, J. H.; Zandbergen, H. W.; Dekker, C. *Phys. Rev. E: Stat., Nonlinear, Soft Matter Phys.* **2005**, *71* (5 Pt 1), 051903.